Time Frequency Localization of Pulse Shaping Filters in OFDM/OQAM Systems

Jinfeng Du, and Svante Signell, Senior Member, IEEE
Department of Electronic, Computer, and Software Systems
KTH - Royal Institute of Technology, Stockholm, Sweden
Email: {jinfeng, srs}@kth.se

***Abstract*— In this paper we investigate the time frequency localization (TFL) properties of different pulse shapes in OFDM/OQAM systems. Various prototype functions, such as rectangular, half cosine, Isotropic Orthogonal Transfer Algorithm (IOTA) function and Extended Gaussian Functions (EGF) are discussed and implemented in a Matlab/Octave Simulation Workbench for Software Defined Radio by direct discretisation of the continuous time model. Simulation results show that pulse shapes with good TFL properties can have near perfect reconstruction.**

I. Introduction

Pulse shaping OFDM/OQAM systems [1]–[3] can achieve smaller combination of inter-symbol and inter-carrier interference (ISI/ICI) without adding any cyclic prefix compared to classic OFDM systems. Various pulse shaping prototype functions with *good* TFL property have been proposed [4]–[7] and implementation issues based on filter banks have been addressed [8]–[10]. Contrary to the classic OFDM scheme which modulates each sub-carrier with a complex-valued symbol, OFDM/OQAM modulates a real-valued symbol in each sub-carrier and consequently allows time-frequency well localized pulse shape under strict TFL requirement [11]. This enables a very efficient way to package symbols that maximizes the throughput or enhances interference robustness in the communication link. OFDM/OQAM has already been introduced in the TIA's Digital Radio Technical Standards [12] and is considered in WRAN (IEEE 802.22) [13].

The transmitted signal in pulse shaping OFDM/OQAM systems can be written in the following analytic form

$$s(t) = \sum_{n=-\infty}^{+\infty} \sum_{m=0}^{N-1} a_{m,n} g_{m,n}(t) \qquad (1)$$

where $a_{m,n}(n \in \mathbb{Z}, m = 0, 1, ..., N-1)$ denotes the real valued symbols conveyed by the sub-carrier of index m during the symbol time of index n, and $g_{m,n}(t)$ represents the synthesis basis which is obtained by the time-frequency translated version of the prototype function $g(t)$ in the following way

$$g_{m,n}(t) = e^{j(m+n)\pi/2} e^{j2\pi m\nu_0 t} g(t - n\tau_0),\ \nu_0\tau_0 = 1/2. \qquad (2)$$

A modified inner product for demodulation is defined as follows

$$\langle x, y \rangle_{\mathbb{R}} = \Re \left\{ \int_{\mathbb{R}} x^*(t) y(t) dt \right\}$$

where $\Re\{\bullet\}$ is the real part operator. It decomposes the lattice points $g_{m,n}$ into four sub-lattices [4]: **EE**=$\{m$ even, n even$\}$, **EO**=$\{m$ even, n odd$\}$, **OE**=$\{m$ odd, n even$\}$ and **OO**=$\{m$ odd, n odd$\}$, as shown in Fig. 1.

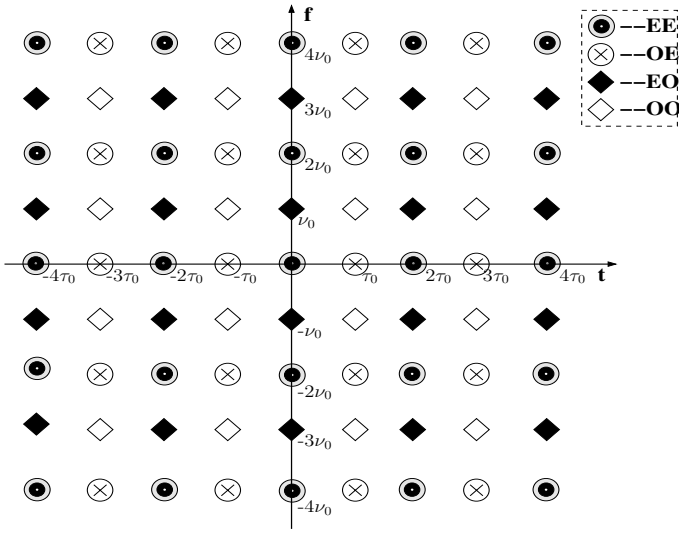

Fig. 1. OFDM/OQAM Lattice.

The orthogonality between different sub-lattices is automatically guarantied and is independent of the prototype function as long as this function is even. While inside the same sub-lattice, the orthogonality can be ensured by finding an even prototype function whose ambiguity function $A_g(\tau, \nu)$ (see (9)) satisfies

$$A_g(2p\tau_0, 2q\nu_0) = \begin{cases} 1, & \text{when } (p,q) = (0,0) \\ 0, & \text{when } (p,q) \neq (0,0) \end{cases} \quad p, q \in \mathbb{Z} \qquad (3)$$

Two kinds of realizations of pulse shaping OFDM/OQAM systems are of practical interest as they are very easy to be implemented in the classic OFDM system. Assume T is the OFDM symbol duration and F is the inter-carrier frequency spacing, we have $TF = 1$ when no cyclic prefix is added. One can either set $\nu_0 = F$ and shorten symbol duration [10], or set

This work was supported in part by Wireless@KTH.

$\tau_0 = T$ and double the number of sub-carriers [9]. We use the former approach.

The paper is organized as follows. Section II presents pulse shape prototypes and introduces criteria for the TFL property. The continuous and discrete time system models and the direct implementation method are introduced in Section III. Simulation results both on TFL and perfect reconstruction are presented in Section IV and conclusions are drawn in Section V

II. Pulse Shape Prototypes and TFL

In the following part of this section, several different types of pulse shape functions are presented, followed by the Heisenberg parameter ξ as an indicator for the TFL property.

A. Prototype Functions

1) Rectangular Function:

$$g(t) = \begin{cases} \frac{1}{\sqrt{2\tau_0}}, & |t| \leq \tau_0 \\ 0, & \text{elsewhere} \end{cases} \tag{4}$$

2) Half Cosine Function:

$$g(t) = \begin{cases} \frac{1}{\sqrt{\tau_0}} \cos \frac{\pi t}{2\tau_0}, & |t| \leq \tau_0 \\ 0, & \text{elsewhere} \end{cases} \tag{5}$$

3) Extended Gaussian Function and IOTA:

$$z_{\alpha,\nu_0,\tau_0}(t) = \frac{1}{2}\left[\sum_{k=0}^{\infty} d_{k,\alpha,\nu_0}\left[g_\alpha(t+\frac{k}{\nu_0}) + g_\alpha(t-\frac{k}{\nu_0})\right]\right] \cdot \sum_{l=0}^{\infty} d_{l,1/\alpha,\tau_0} \cos(2\pi l \frac{t}{\tau_0}) \tag{6}$$

where $\tau_0\nu_0 = \frac{1}{2}$, $0.528\nu_0^2 \leq \alpha \leq 7.568\nu_0^2$, d_{k,α,ν_0} are real valued coefficients and can be computed via the rules described in [4], [8]. This family of functions are named as Extended Gaussian Function (EGF) as they are derived from the Gaussian function g_α which is defined by

$$g_\alpha(t) = (2\alpha)^{1/4} e^{-\pi\alpha t^2}, \ \alpha > 0 \tag{7}$$

Note that, for EGF and Gaussian functions, their Fourier transforms have the same shape as themselves except for an axis scaling factor [8]

$$\mathcal{F} z_{\alpha,\nu_0,\tau_0}(t) = z_{1/\alpha,\tau_0,\nu_0}(f), \quad \mathcal{F} g_\alpha(f) = g_{1/\alpha}(f) \tag{8}$$

A special case of EGF, $\zeta(t) = z_{1,\frac{1}{\sqrt{2}},\frac{1}{\sqrt{2}}}(t)$, is called Isotropic Orthogonal Transform Algorithm (IOTA) Function due to its invariance to Fourier transform $\mathcal{F}\zeta(t) = \zeta(f)$.

B. Ambiguity Function and Heisenberg Parameter

The (auto-)ambiguity function is defined as

$$A_g(\tau,\nu) = \int_{\mathbb{R}} e^{-j2\pi\nu t} g(t+\tau/2) g^*(t-\tau/2) dt \tag{9}$$

and the Heisenberg parameter [1] $\xi = \frac{1}{4\pi\Delta t\Delta f} \leq 1$ where

$$\begin{cases} (\Delta t)^2 & = \int_{\mathbb{R}} t^2 |g(t)|^2 dt \\ (\Delta f)^2 & = \int_{\mathbb{R}} f^2 |G(f)|^2 df \end{cases} \tag{10}$$

in which $g(t)$ is assumed to be origin-centered with unity energy [14] for simple expression. Δt is the mass moment of inertia of the prototype function in time and Δf in frequency, which indicates how the energy (mass) of the prototype function spreads over the time and frequency plane. According to the Heisenberg uncertainty inequality [15], $0 \leq \xi \leq 1$, where the upper bound $\xi = 1$ is achieved by the Gaussian function and the lower band $\xi = 0$ is achieved by the rectangular function whose Δf is infinite. The larger ξ is, the better joint time-frequency localization the prototype function has.

III. System Implementation

Rather than deriving the implementation structure from filterbank theory, like in [8]–[10], we try to find an implementation method by direct discretisation of the continuous time model without considering the perfect reconstruction (PR) condition.

Let $s(t)$ be the output signal of the OFDM/OQAM modulator

$$s(t) = \sum_{n=-\infty}^{\infty} \sum_{m=0}^{N-1} (a_{m,n}^{\Re} g_{m,2n}(t) + a_{m,n}^{\Im} g_{m,2n+1}(t)), \tag{11}$$

the demodulated signal at branch k during symbol duration n can be written as

$$\begin{aligned} \tilde{a}_{m,n}^{\Re} &= \Re\left\{\int_{\mathbb{R}} s(t) g_{m,2n}^*(t) dt\right\} \\ \tilde{a}_{m,n}^{\Im} &= \Re\left\{\int_{\mathbb{R}} s(t) g_{m,2n+1}^*(t) dt\right\} \end{aligned} \tag{12}$$

where $\Re$ and $\Im$ indicate the real and imaginary part respectively. By sampling $s(t)$ at rate $1/T_s$ during time interval $[nT - \tau_0, nT + \tau_0)$, we get

$$\begin{aligned} s(nT + kT_s) = \sum_{l=-\infty}^{\infty} \sum_{m=0}^{N-1} \big[& a_{m,l}^{\Re} g(nT + kT_s - lT) \\ & + j a_{m,l}^{\Im} g(nT + kT_s - lT - \frac{T}{2}) \Big] e^{j\frac{\pi}{2}(m+2l)} e^{j2\pi\frac{mk}{N}} \end{aligned} \tag{13}$$

where $n \in \mathbb{Z}$ and $k = -\frac{N}{2}, ..., \frac{N}{2} - 1$.

Let $s_k[n] = s[nN + k] = s(nT + kT_s)$, and rewrite (13) as

$$\begin{aligned} s_k[n] &= \sum_p g(pT + kT_s) \left[\sum_{m=0}^{N-1} a_{m,n-p}^{\Re} e^{j\frac{\pi}{2}(m+2n-2p)} e^{j2\pi\frac{mk}{N}}\right] \\ &+ \sum_p g(pT + kT_s - \frac{T}{2}) \left[\sum_{m=0}^{N-1} j a_{m,n-p}^{\Im} e^{j\frac{\pi}{2}(m+2n-2p)} e^{j2\pi\frac{mk}{N}}\right] \\ &= \sum_p \left[g_k[p] A_N^k(a_{m,n-p}^{\Re}) + g_{k-N/2}[p] A_N^k(j a_{m,n-p}^{\Im})\right] \\ &= g_k[n] * A_N^k(a_{m,n}^{\Re}) + g_{k-N/2}[n] * A_N^k(j a_{m,n}^{\Im}) \end{aligned} \tag{14}$$

where

$$A_N^k(x_{m,n}) = \sum_{m=0}^{N-1} x_{m,n} e^{j\frac{\pi}{2}(m+2n)} e^{j2\pi\frac{mk}{N}} \tag{15}$$

$$g_k[n] = g[nN + k] = g(nT + kT_s) \tag{16}$$

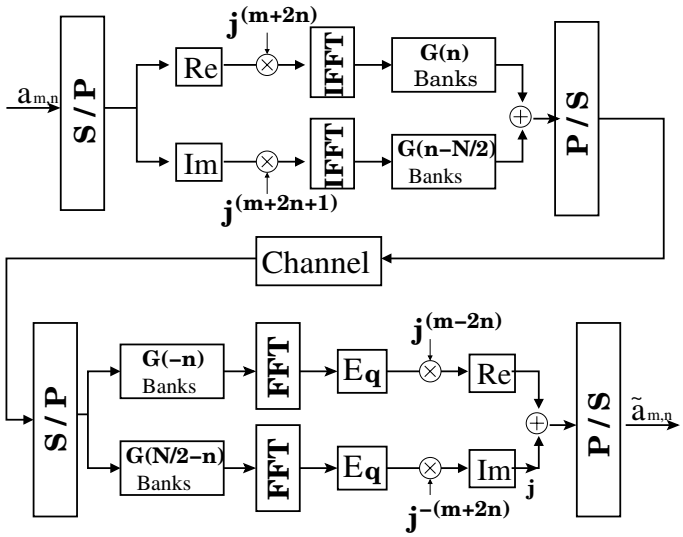

Fig. 2. Implementation diagram.

Therefore the OFDM/OQAM modulator can be easily implemented by an IFFT block defined in (15) followed by a bank of component filters which are obtained by partitioning the polyphase representation of $g(t)$ in the way defined in (16).

At the receiver side, we sample the received signal $r(t)$ at rate $1/T_s$, and rewrite the integration in (12) via approximation

$$\begin{aligned}
\tilde{a}^{\Re}_{m,n} &\approx \Re\left\{ T_s \sum_{l=-\infty}^{\infty} \sum_{k=-\frac{N}{2}}^{\frac{N}{2}-1} r(lT+kT_s) g^*_{m,2n}(lT+kT_s) \right\} \\
&= \Re\left\{ T_s e^{-j\frac{\pi}{2}(m+2n)} \sum_{k=-\frac{N}{2}}^{\frac{N}{2}-1} \sum_{l=-\infty}^{\infty} r_k[l] g_k[l-n] e^{-j2\pi\frac{mk}{N}} \right\} \\
&= \Re\left\{ T_s e^{-j\frac{\pi}{2}(m+2n)} \sum_{k=-\frac{N}{2}}^{\frac{N}{2}-1} r_k[n] * g_k[-n] e^{-j2\pi\frac{mk}{N}} \right\} \quad (17) \\
&= \Re\left\{ T_s e^{j\frac{\pi}{2}(m-2n)} \sum_{k=-\frac{N}{2}}^{\frac{N}{2}-1} r_k[n] * g_k[-n] e^{-j2\pi\frac{m(k+N/2)}{N}} \right\}
\end{aligned}$$

$$\tilde{a}^{\Im}_{m,n} \approx \Im\left\{ T_s e^{-j\frac{\pi}{2}(m+2n)} \sum_{k=-\frac{N}{2}}^{\frac{N}{2}-1} r_k[n] * g_{k-\frac{N}{2}}[-n] e^{-j2\pi\frac{mk}{N}} \right\}$$

where $g_k[-n] = g[-nN+k] = g(-NT+kT_s)$. Similarly, the OFDM/OQAM demodulator can be implemented by filter component banks $g_k[n]$ and $g_{k-\frac{N}{2}}[n]$ followed by an FFT block. The implementation diagram is shown in Fig. 2, which looks similar as the system diagram presented in [16].

Assume the pulse shape prototype function $g(t)$ (or its truncation) has finite duration in $-M\tau_0 \le t \le M\tau_0$, its discrete version $g[n]$ is nonzero when $n = -MN/2, ..., MN/2$, and therefore the length of $g[n]$ will be $MN+1$. In order to have the same number of taps in each component filter, we just drop the last sample of $g[n]$ so that the length of each component filter equals to M.

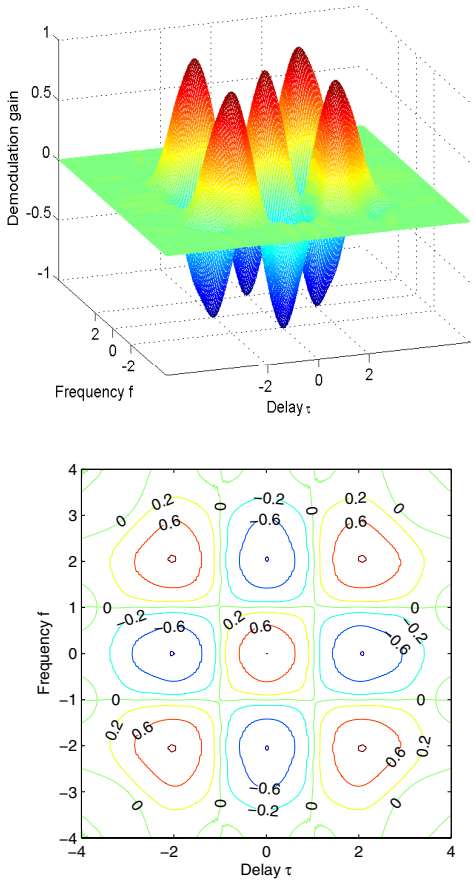

Fig. 3. Demodulation gain of OFDM/OQAM system.

IV. Numerical Results

A. Time Frequency Localization (TFL)

To illustrate how the demodulation gain varies with respect to the time and frequency spread, the ambiguity function of the output of one demodulation branch is plotted both in a three dimensional plot and a two-dimension contour plot, as shown in Fig. 3, in which the IOTA prototype function is used and axes are normalized by τ_0 and ν_0 respectively.

Here the data transmitted on each basis function is ignored for simplicity, and only the neighboring lattice points in the same subset are considered. Those pulses on lattice points with distance $2\tau_0$ or $2\nu_0$ have negative envelope due to the phase factor $e^{j\frac{\pi}{2}(m+n)}$ which equals to -1 when either $|m|$ or $|n|$ equals to 2, but not both. 0 is achieved at the boundary of each lattice grid and therefore no interference will be introduced by neighbors as long as the normalized time or frequency dispersion is less than 2.

The Heisenberg parameter ξ for each pulse is calculated with $\frac{\tau_0}{T} = \frac{\nu_0}{F}$, see Table I. For each normalized time or frequency unit, 32 samples are used.

The Gaussian pulse achieves the maximum of $\xi = 1$ and therefore has the best TFL property. The IOTA pulse shows satisfying localization which maximizes ξ among the EGF functions [4]. One thing has to be noticed is that the IOTA

TABLE I

THE HEISENBERG PARAMETER ξ

$t, f \in$	Rect[a]	HalfCosine	Gauss	IOTA	EGF[b] $\alpha = 3.774$
$[-6, 6]$	0.3518	0.8949	1.000	0.9769	0.7015
$[-40, 40]$	0.1028	0.8705	1.000	0.9769	0.6878

[a] for rectangular pulse, $(\Delta f)^2 = \int f^2 \text{sinc}^2(wf)df = \infty$ and therefore $\xi = 0$ in theory.

[b] for EGF pulse, $\xi(\alpha) = \xi(1/\alpha)$ and it will steadily increase to its maximum as α approaches 1 from either direction.

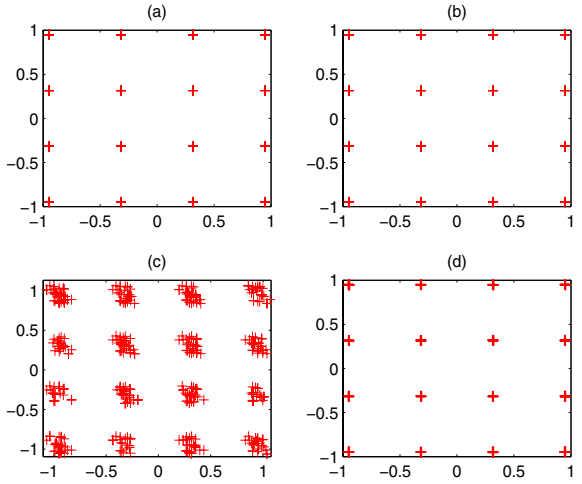

Fig. 4. Signal constellation with 16QAM modulation for (a) EGF (b) Half Cosine (c) Rectangular (d) Root Raised Cosine with $\rho = 0.2$.

prototype function will not be used in our implementation as we have to set $\frac{\tau_0}{T} = 1/2$ and $\frac{\nu_0}{F} = 1$, rather than what is demanded in IOTA function where $\frac{\tau_0}{T} = \frac{\nu_0}{F} = 1/\sqrt{2}$.

B. Simulation in the SDR Workbench

We have implemented the pulse shaping OFDM/OQAM system in the Matlab/Octave simulation workbench [17]. The FFT/IFFT size is 64 for all the following simulations. As stated in Section III, the pulse shape prototype function $g(t)$ is truncated (if necessary) to a finite duration $-M\tau_0 \leq t < M\tau_0$.

Fig. 4 presents the reconstructed signal constellation at the OFDM/OQAM demodulator output for an ideal channel. With the length of component filters $M = 12$, EGF, Half Cosine and Root Raised Cosine prototypes can achieve almost perfect reconstruction (see Fig. 4 a, b, d) while the Rectangular prototype will result in some distorsion (see Fig. 4 c).

For the EGF prototype function, three parameters will affect its performance: α, τ_0 and the length of filter taps M. Fig. 5 displays the influence of α and M. It shows that when the number of filter taps is large enough (e.g. $M = 6$), the performance of EGF prototypes with different α is pretty good. However, when the number of filter taps is insufficient (e.g. $M = 2$), the most centralized prototype (with highest α) will be least affected by truncation (cf. Fig. 5 b vs. Fig. 5 d).

Fig. 6 displays the influence of the symbol length τ_0 on reconstruction performance with fixed $\alpha = 2$ and M.

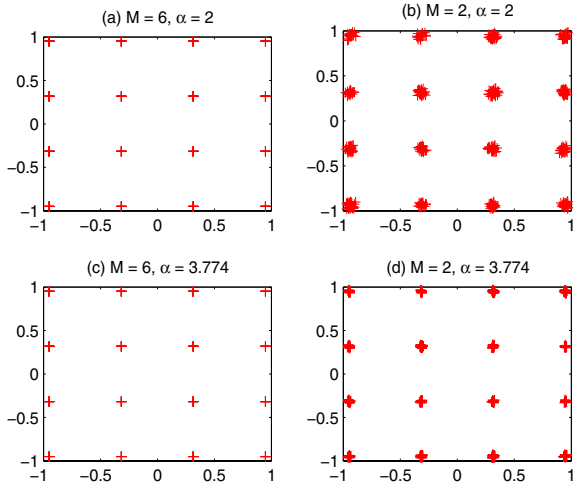

Fig. 5. Signal constellation of EGF with 16QAM modulation.

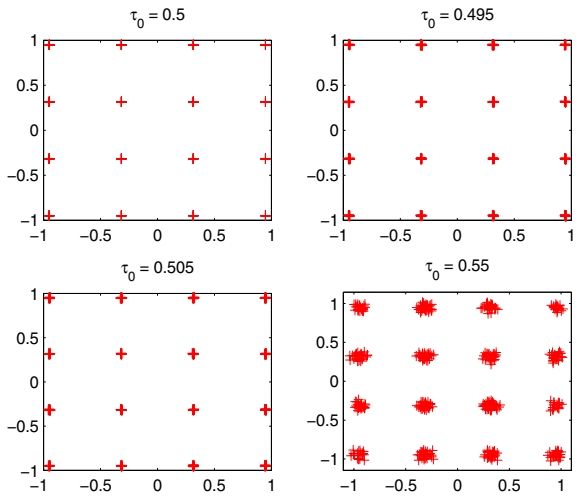

Fig. 6. Signal constellation of EGF with 16QAM modulation for $M = 6$, $\alpha = 2$ with different τ_0.

Obviously even a slight variation of τ_0 affects the performance significantly.

V. CONCLUSIONS

The time frequency localization properties indicated by the Heisenberg parameter, the Ambiguity function, as well as the interference function and the instantaneous correlation functions [14] provide an intuitive way to describe how signals from different carriers and different symbols get along with each other. As the transmitted signal composed by basis functions will place a copy of the prototype function on each lattice point in the time-frequency plane, the less power the prototype function spreads to the neighboring lattice region, the better reconstruction of the transmitted signal can be retrieved after demodulation.

By adaptively exploiting different prototype functions with

varying TFL properties, dynamic spectrum allocation can be achieved in a more natural way, since the transmitter and receiver adapts dynamically to different channel conditions and interference environments leading to a higher reliability and spectral efficiency can be expected. Also simplified synchronization can be expected as less sensitivity to time and frequency offset is achieved. Therefore, OFDM/OQAM is a promising candidate in the future wireless communication.

REFERENCES

[1] B. le Floch, M. Alard and C. Berrou, "Coded Orthogonal Frequency Division Multiplex," *Proceedings of the IEEE*, vol. 83, pp. 982–996, June 1995.

[2] H. Bölcskei, P. Duhamel, and R. Hleiss, "Design of pulse shaping OFDM/OQAM systems for high data-rate transmission over wireless channels," in Proc. of *IEEE International Conference on Communications (ICC)*, Vancouver, BC, Canada, June 1999, vol. 1, pp. 559–564.

[3] D. Schafhuber, G. Matz, and F. Hlawatsch, "Pulse-shaping OFDM/BFDM systems for time-varying channels: ISI/ICI analysis, optimal pulse design, and efficient implementation," in Proc. of *IEEE International Symposium on Personal, Indoor and Mobile Radion Communications*, Lisbon, Portugal, Sep. 2002, pp. 1012–1016.

[4] M. Alard, C. Roche, and P. Siohan, "A new family of function with a nearly optimal time-frequency localization," *Technical Report of the RNRT Project Modyr*, 1999.

[5] N.J. Baas and D.P. Taylor, "Pulse shaping for wireless communication over time- or frequency-selective channels", *IEEE Transactions on Communications*, vol 52, pp. 1477–1479, Sep. 2004.

[6] A. Vahlin and N. Holte, "Optimal finite duration pulse for OFDM," *IEEE Transactions on Communications*, vol. 44, pp. 10–14, Jan. 1996.

[7] R. Haas and J.-C. Belfiore, "A time-frequency well-localized pulse for multiple carrier transmission," *Wireless Personal Communications*, vol. 5, pp. 1–18, Jan. 1997.

[8] P. Siohan and C. Roche, "Cosine-Modulated Filterbanks Based on Extended Gaussian Function", *IEEE Transactions on Signal Processing*, vol. 48, no. 11, pp. 3052–3061, Nov. 2000.

[9] L. Vangelista and N. Laurenti, "Efficient Implementations and Alternative Architectures for OFDM-OQAM Systems", *IEEE Transactions on Communications*, vol. 49, no. 4, pp. 664–675, Apr. 2001.

[10] P. Siohan, C. Siclet and N. Lacaille, "Analysis and design of OFDM/OQAM. systems based on filterbank theory", *IEEE Transactions on Signal Processing*, vol. 50, no. 5, pp. 1170–1183, May 2002.

[11] H. Bölcskei, "Orthogonal Frequency Division Multiplexing Based on Offset-QAM", *Advances in Gabor Analysis*, Birkhäuser, 2003.

[12] TIA Committee TR-8.5, "Wideband Air Interface Isotropic Orthogonal Transform Algorithm (IOTA) –Public Safety Wideband Data Standards Project – Digital Radio Technical Standards," TIA-902.BBAB (Physical Layer Specification, Mar. 2003) and TIA-902.BBAD (Radio Channel Coding (CHC) Specification, Aug. 2003) http://www.tiaonline.org/standards/

[13] M. Bellec and P. Pirat, "OQAM performances and complexity," *IEEE P802.22 Wireless Regional Area Network (WRAN)*, Jan. 2006. http://www.ieee802.org/22/Meeting_documents/2006_Jan/22-06-0018-01-0000_OQAM_performances_and_complexity.ppt

[14] J. Du and S. Signell, "Classic OFDM Systems and Pulse Shaping OFDM/OQAM Systems", *Technical Report of the Wireless@KTH Project Next Generation FDM*, TRITA-ICT/ECS R 07:01, Feb. 2007.

[15] S. Mallat, *A Wavelet Tour of Signal Processing, Second Edition*, Academic Press, 1999.

[16] B. Hirosaki, "An Orthogonally Multiplexed QAM System Using the Discrete Fourier Transform", *IEEE Transactions on Communications*, vol. 29, no. 7, pp. 982–989, Jul. 1981.

[17] S. Signell and J. Huang, "A Matlab/Octave Simulation Workbench for Multi-Antenna Software Defined Radio", in Proc. of *24th Norchip Conference*, Linköping, Sweden, November 2006, pp. 145–148